# Comparative Study of Sensorless Methods Based on Sliding Mode Observer for Dual Three-Phase Permanent Magnet Synchronous Machine

Linhui Fan, Tao Yang, Yuzheng Chen, Serhiy Bozhko
*Department of Electrical and Electronics Engineering, University of Nottingham, Nottingham, UK*
Email: Linhui.Fan@nottingham.ac.uk

***Abstract*—In recent years, increased attentions have been given to multiphase electrical machines because of their fault tolerance ability which is quite important for more-electric aircraft application. A dual three-phase PMSM for turboprop aircraft green taxiing green-taxiing/generator applications is developed in this paper. And a sensorless control is designed for this system to satisfy the space requirement of the manufacturer. Firstly, the mathematical model of the machine is illustrated. Then the conventional sliding-mode control based sensorless method is introduced. To eliminate the phase delay caused by the low-pass filter and improve the dynamic performance of the conventional method, the adaptive method is adopted. Afterwards, s-domain simulations in the Matlab/Simulink are conducted to compare the performance of these two approaches. The simulation results show that the adaptive method has better dynamic performance and lower steady state error than the conventional method. While, conventional method has inferior but acceptable performance.**

***Keywords—More-Electric Aircraft, Dual Three-Phase PMSM, Sensorless Control, Sliding-Mode Observer.***

## I. INTRODUCTION

Multiphase electric machines have been applied to more-electric aircraft (MEA) application in recent years with increasing interest [1]. The growing interest in multiphase machines is due to their notable improvements when compared with their conventional three-phase counterparts. For instance, multiphase machines have lower torque pulsations, less dc-link current, reduced rotor harmonic currents, higher power per ampere ratio for the same machine volume [2]. A dual three-phase PMSM machine is investigated in this paper to check whether it could increase the redundancy and fault-tolerant ability of the system. As shown in Fig.1, this machine consists of two star-connected three-phase stator windings with two isolated neutral points. To combat the size limitation of installing mechanical speed/position sensors in the airplane gear box, sensorless control is adopted since it could save space as well as installation cost and improve the reliability of the system simultaneously.

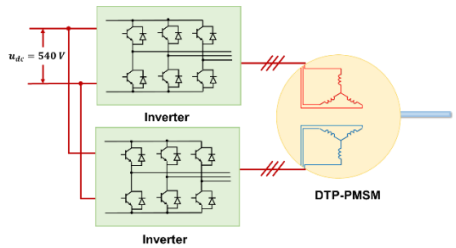


Fig. 1 Block diagram of DTP-PMSM drive system. [3]

Sensorless control methods can be categorized into two major groups [4]: the back EMF based method [5] and the saliency tracking based method [6]. Among various methods, the sliding-mode control (SMO) method, as a practical instance of rotor speed/position estimation, is widely used because of its simple algorithm and robustness [7]. This study made efforts to fill the gap in the research of sensorless control to multiphase machines to some extent although the sensorless control is not a completely innovate idea and has been studied for several decades. In this paper, the mathematical model of dual three-phase PMSM machine is firstly built. Then two different SMO methods are introduced (conventional SMO method and the adaptive SMO method). Afterwards, a comparison of the simulation results of these two methods is made and relating conclusion is given at last.

## II. DUAL THREE-PHASE PMSM MODEL

The DTP-PMSM in this study consists of two sets of three-phase windings. Each set is designed to shift from the other by 180 electrical degrees. According to the mathematical model of the machine detailed in [5], the voltage equation in $\alpha\beta$ stationary frame can be deduced as:

$$\begin{bmatrix} u_{\alpha_{1,2}} \\ u_{\beta_{1,2}} \end{bmatrix} = M_0 \begin{bmatrix} i_{\alpha_{1,2}} \\ i_{\beta_{1,2}} \end{bmatrix} + \begin{bmatrix} e_{\alpha_{1,2}} \\ e_{\beta_{1,2}} \end{bmatrix} \quad (1)$$

where

$$M_0 = \begin{bmatrix} R + \frac{d}{dt}L_D & -\omega_e L_Q \\ \omega_e L_Q & R + \frac{d}{dt}L_D \end{bmatrix}$$

The extended EMF in stationary frame can be expressed as:

$$\begin{bmatrix} e_{\alpha_{1,2}} \\ e_{\beta_{1,2}} \end{bmatrix} = e \begin{bmatrix} -sin\theta_e \\ cos\theta_e \end{bmatrix} \quad (2)$$

## III. SLIDING-MODE OBSERVER BASED SENSORLESS CONTROL

The information of rotor position is contained in the extended EMF as shown in (2). To obtain the estimated rotor position, the extended EMF will be estimated first. Two estimation methods are studied in this session, i.e., conventional method and adaptive method. After obtaining the estimated extended EMF, speed and position of rotor are estimated using arctan function and PLL based estimator, respectively.

### *A. Estimation of Back-EMF*

#### *1) Conventional Method*

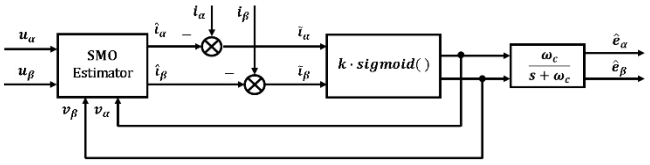


Fig. 2 Block diagram of conventional SMO method.

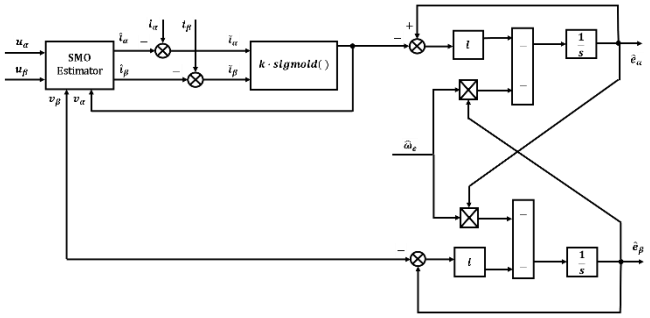


Fig. 3 Block diagram of adaptive SMO method

To make the derivation simpler, the mathematical model of DTP-PMSM in $\alpha\beta$ stationary frame can be rewritten as state equation of the current:

$$\frac{d}{dt}\begin{bmatrix} i_{\alpha_{1,2}} \\ i_{\beta_{1,2}} \end{bmatrix} = M_1 \begin{bmatrix} i_{\alpha_{1,2}} \\ i_{\beta_{1,2}} \end{bmatrix} + \frac{1}{L_D}\begin{bmatrix} u_{\alpha_{1,2}} \\ u_{\beta_{1,2}} \end{bmatrix} - \frac{1}{L_D}\begin{bmatrix} e_{\alpha_{1,2}} \\ e_{\beta_{1,2}} \end{bmatrix} \quad (3)$$

where

$$M_1 = \frac{1}{L_D}\begin{bmatrix} -R & \omega_e L_Q \\ -\omega_e L_Q & -R \end{bmatrix}$$

The sliding-mode observer in Fig.2 is designed as:

$$\frac{d}{dt}\begin{bmatrix} \hat{\imath}_{\alpha_{1,2}} \\ \hat{\imath}_{\beta_{1,2}} \end{bmatrix} = M_5 \begin{bmatrix} \hat{\imath}_{\alpha_{1,2}} \\ \hat{\imath}_{\beta_{1,2}} \end{bmatrix} + \frac{1}{L_D}\begin{bmatrix} u_{\alpha_{1,2}} \\ u_{\beta_{1,2}} \end{bmatrix} - \frac{1}{L_D}\begin{bmatrix} v_{\alpha_{1,2}} \\ v_{\beta_{1,2}} \end{bmatrix} \quad (4)$$

Usually, a sign function is applied to obtain $v_{\alpha_{1,2}}$ and $v_{\beta_{1,2}}$ from current error as shown in (5).

$$\begin{bmatrix} v_{\alpha_{1,2}} \\ v_{\beta_{1,2}} \end{bmatrix} = \begin{bmatrix} k \cdot sign(\hat{\imath}_{\alpha_{1,2}} - i_{\alpha_{1,2}}) \\ k \cdot sign(\hat{\imath}_{\beta_{1,2}} - i_{\beta_{1,2}}) \end{bmatrix} \quad (5)$$

where *k* is a constant observer gain which meets the following requirement:

$$k > \max\{|e_{\alpha_{1,2}}|, |e_{\beta_{1,2}}|\} \quad (6)$$

*sign*(*x*) is the sign function and has the following expression:

$$sign(x) = \begin{cases} -1 & x < 0 \\ 0 & x = 0 \\ 1 & x > 0 \end{cases}$$

According to [7], the chattering phenomenon caused by the discontinuity of sign function can be reduced if it is replaced by the sigmoid function which can be expressed as:

$$sigmoid(x) = \frac{2}{1+e^{-ax}} - 1 \quad (7)$$

where *a* is an adjustable parameter.

The current error equation is obtained as (8) by subtracting (4) from (3).

$$\frac{d}{dt}\begin{bmatrix} \tilde{\imath}_{\alpha_{1,2}} \\ \tilde{\imath}_{\beta_{1,2}} \end{bmatrix} = M_5 \begin{bmatrix} \tilde{\imath}_{\alpha_{1,2}} \\ \tilde{\imath}_{\beta_{1,2}} \end{bmatrix} + \frac{1}{L_D}\begin{bmatrix} e_{\alpha_{1,2}} - v_{\alpha_{1,2}} \\ e_{\beta_{1,2}} - v_{\beta_{1,2}} \end{bmatrix} \quad (8)$$

where

$$\begin{cases} \tilde{\imath}_{\alpha_{1,2}} = \hat{\imath}_{\alpha_{1,2}} - i_{\alpha_{1,2}} \\ \tilde{\imath}_{\beta_{1,2}} = \hat{\imath}_{\beta_{1,2}} - i_{\beta_{1,2}} \end{cases} \quad (9)$$

According to the sliding-mode variable structure theory [7], the sliding surface is defined as:

$$S(X) = \begin{bmatrix} S_\alpha(X) \\ S_\beta(X) \end{bmatrix} = \begin{bmatrix} \tilde{\imath}_{\alpha_{1,2}} \\ \tilde{\imath}_{\beta_{1,2}} \end{bmatrix} \quad (10)$$

Once the system reaches the sliding surface, there exists:

$$\frac{d}{dt}S(X) = S(X) = 0 \quad (11)$$

Hence,

$$\frac{d}{dt}\begin{bmatrix} \tilde{\imath}_{\alpha_{1,2}} \\ \tilde{\imath}_{\beta_{1,2}} \end{bmatrix} = \begin{bmatrix} \tilde{\imath}_{\alpha_{1,2}} \\ \tilde{\imath}_{\beta_{1,2}} \end{bmatrix} = 0 \quad (12)$$

Based on equivalent control method, substituting (8) into (12) yields,

$$\begin{bmatrix} e_{\alpha_{1,2}} \\ e_{\beta_{1,2}} \end{bmatrix} = \begin{bmatrix} v_{\alpha_{1,2}} \\ v_{\beta_{1,2}} \end{bmatrix} = \begin{bmatrix} k \cdot sigmoid(\hat{\imath}_{\alpha_{1,2}} - i_{\alpha_{1,2}}) \\ k \cdot sigmoid(\hat{\imath}_{\beta_{1,2}} - i_{\beta_{1,2}}) \end{bmatrix} \quad (13)$$

To prove the stability of (5), the Lyapunov function can be defined as [7]:

$$V = \frac{1}{2}S(X)^T S(X) = \frac{1}{2}(S_\alpha^2(X) + S_\beta^2(X)) \quad (14)$$

Differentiating (14) gives

$$\frac{d}{dt}V = S_\alpha(X)\frac{d}{dt}S_\alpha(X) + S_\beta(X)\frac{d}{dt}S_\beta(X) \quad (15)$$

Substituting (8) and (9) into (15) yields

$$\frac{d}{dt}V = \frac{1}{L_D}\left[e_{\alpha_{1,2}}\tilde{\imath}_{\alpha_{1,2}} - k \cdot sigmoid(\tilde{\imath}_{\alpha_{1,2}})\tilde{\imath}_{\alpha_{1,2}}\right] + \frac{1}{L_D}\left[e_{\beta_{1,2}}\tilde{\imath}_{\beta_{1,2}} - k \cdot sigmoid(\tilde{\imath}_{\beta_{1,2}})\tilde{\imath}_{\beta_{1,2}}\right] - \frac{R}{L_D}(\tilde{\imath}_{\alpha_{1,2}}^2 + \tilde{\imath}_{\beta_{1,2}}^2) \quad (16)$$

Substitute (6) into (16) giving $\frac{d}{dt}V \le 0$, hence the the stability of conventional method can be verified.

*2) Adaptive Method*

For surface-mounted machine, the extended EMF shown in (2) can be simplified to

$$\begin{bmatrix} e_{\alpha_{1,2}} \\ e_{\beta_{1,2}} \end{bmatrix} = \omega_e \varphi_m \begin{bmatrix} -sin\theta_e \\ cos\theta_e \end{bmatrix} \quad (17)$$

Since the change of rotor speed is far slower than that of current, the rotor speed can be assumed not to vary during one estimation cycle, i.e., $\frac{d}{dt}\omega_e = 0$. Hence, the derivative equation of (17) can be written as

$$\frac{d}{dt}\begin{bmatrix} e_{\alpha_{1,2}} \\ e_{\beta_{1,2}} \end{bmatrix} = \omega_e \begin{bmatrix} -e_{\beta_{1,2}} \\ e_{\alpha_{1,2}} \end{bmatrix} \quad (18)$$

Basing on (18), an extended EMF observer is built as

$$\begin{cases} \frac{d}{dt}\hat{e}_{\alpha_{1,2}} = -\hat{\omega}_e\hat{e}_{\beta_{1,2}} - l(\hat{e}_{\alpha_{1,2}} - e_{\alpha_{1,2}}) \\ \frac{d}{dt}\hat{e}_{\beta_{1,2}} = \hat{\omega}_e\hat{e}_{\alpha_{1,2}} - l(\hat{e}_{\beta_{1,2}} - e_{\beta_{1,2}}) \\ \frac{d}{dt}\hat{\omega}_e = (\hat{e}_{\alpha_{1,2}} - e_{\alpha_{1,2}})\hat{e}_{\beta_{1,2}} - (\hat{e}_{\beta_{1,2}} - e_{\beta_{1,2}})\hat{e}_{\alpha_{1,2}} \end{cases} \quad (19)$$

where $l$ is the observer gain which is a positive real number.

The error equation of the observer is obtained by subtracting (19) from (18).

$$\begin{cases} \frac{d}{dt}\tilde{e}_{\alpha_{1,2}} = -\hat{\omega}_e\hat{e}_{\beta_{1,2}} + \omega_e e_{\beta_{1,2}} - l\tilde{e}_{\alpha_{1,2}} \\ \frac{d}{dt}\tilde{e}_{\beta_{1,2}} = \hat{\omega}_e\hat{e}_{\alpha_{1,2}} - \omega_e e_{\alpha_{1,2}} - l\tilde{e}_{\beta_{1,2}} \\ \frac{d}{dt}\tilde{\omega}_e = \tilde{e}_{\alpha_{1,2}}\hat{e}_{\beta_{1,2}} - \tilde{e}_{\beta_{1,2}}\hat{e}_{\alpha_{1,2}} \end{cases} \quad (20)$$

where

$$\begin{cases} \tilde{e}_{\alpha_{1,2}} = \hat{e}_{\alpha_{1,2}} - e_{\alpha_{1,2}} \\ \tilde{e}_{\beta_{1,2}} = \hat{e}_{\beta_{1,2}} - e_{\beta_{1,2}} \\ \tilde{\omega}_e = \hat{\omega}_e - \omega_e \end{cases} \quad (21)$$

To prove the stability of (21), the Lyapunov function is defined as [7]

$$V = \frac{1}{2}(\tilde{e}_{\alpha_{1,2}}^2 + \tilde{e}_{\beta_{1,2}}^2 + \tilde{\omega}_e^2) \quad (22)$$

The differential form of (22) can be presented as

$$\frac{d}{dt}V = \tilde{e}_{\alpha_{1,2}}\frac{d}{dt}\tilde{e}_{\alpha_{1,2}} + \tilde{e}_{\beta_{1,2}}\frac{d}{dt}\tilde{e}_{\beta_{1,2}} + \tilde{\omega}_e\frac{d}{dt}\tilde{\omega}_e \quad (23)$$

Substitute (20) into (23) yielding,

$$\frac{d}{dt}V = -l(\tilde{e}_{\alpha_{1,2}}^2 + \tilde{e}_{\beta_{1,2}}^2) \leq 0 \quad (24)$$

Hence, the stability of the adaptive method is verified by (24).

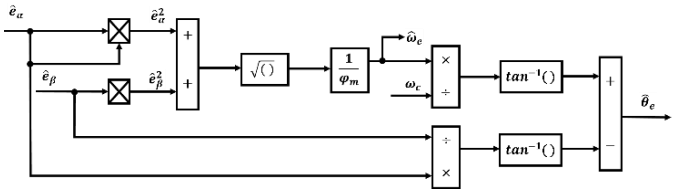


Fig. 4 Block diagram of speed and position estimation using arctan unction.

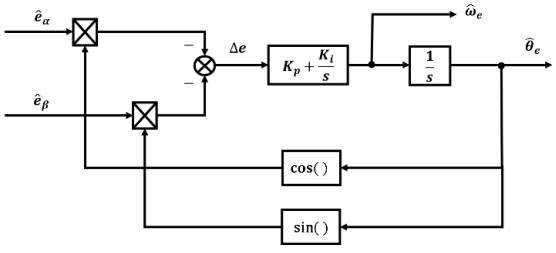


Fig. 5 Block diagram of speed and position estimation using PLL.

## B. Estimation of Rotor Speed and Position

In this section, two different ways for speed and position estimation are compared, i.e., arctan function and Phase-Locked Loop (PLL). The schematic diagrams of both methods are illustrated in Fig. 4 and Fig. 5 respectively.

### 1) Arctan Function.

In the conventional method introduced in section A, a first-order low-pass filter is usually used for filtering as shown in Fig. 2. Hence, the following equation exits.

$$\frac{d}{dt}\begin{bmatrix}\hat{e}_{\alpha_{1,2}} \\ \hat{e}_{\beta_{1,2}}\end{bmatrix} = \begin{bmatrix}(-\hat{e}_{\alpha_{1,2}} + k \cdot sigmoid(\tilde{\imath}_{\alpha_{1,2}}))\omega_c \\ (-\hat{e}_{\beta_{1,2}} + k \cdot sigmoid(\tilde{\imath}_{\beta_{1,2}}))\omega_c\end{bmatrix} \quad (25)$$

where $\omega_c$ is the bandwidth of the low-pass filter.

According to (2), the rotor position can be obtained by estimated extended EMF using arctan function.

$$\hat{\theta}_{eq} = -arctan\left(\frac{\hat{e}_\alpha}{\hat{e}_\beta}\right) \quad (26)$$

Low-pass filter will cause the phase delay which is related to its own cut-off frequency and the angular frequency of the input signal. In order to compensate for the phase delay, a phase compensation part is added to (26) as shown in (27).

$$\hat{\theta}_e = \hat{\theta}_{eq} + arctan\left(\frac{\hat{\omega}_e}{\omega_c}\right) \quad (27)$$

Basing on (17), the estimated rotor speed for surface-mounted machine can be derived as

$$\hat{\omega}_e = \frac{\sqrt{\hat{e}_\alpha^2 + \hat{e}_\beta^2}}{\varphi_m} \quad (28)$$

### 2) PLL Based Estimator

According to (2), the extend EMF error signal $\Delta e$ in Fig. 5 can be presented as:

$$\Delta e = -\hat{e}_\alpha cos\hat{\theta}_e - \hat{e}_\beta sin\hat{\theta}_e = e(sin\theta_e cos\hat{\theta}_e - cos\theta_e sin\hat{\theta}_e) = e \cdot sin(\theta_e - \hat{\theta}_e) \quad (29)$$

The following approximation exists if $\theta_e - \hat{\theta}_e \approx 0\ rad$ [8].

$$\Delta e \approx e(\theta_e - \hat{\theta}_e) \quad (30)$$

Thus, the rotor position error is proportional to $\Delta e$ and a PI controller is applied to correct the position estimation error and make the estimated result converge to the reference one. The details of the design of PLL based estimator could be found in the previous work of author [5].

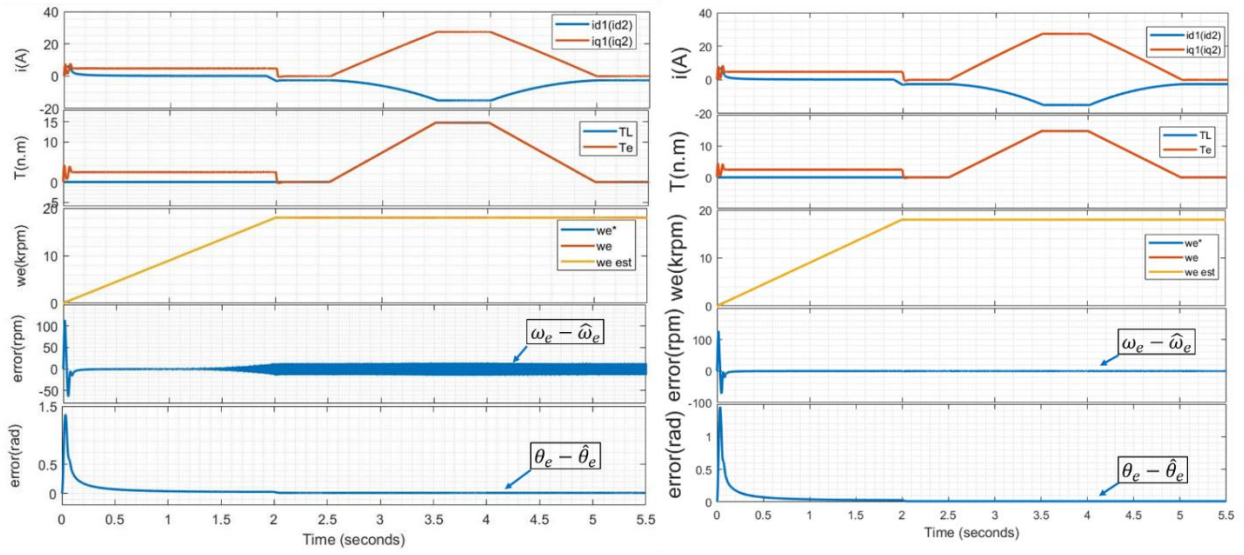


Figure 6 Simulation results (a) conventional SMO method (b) adaptive method.

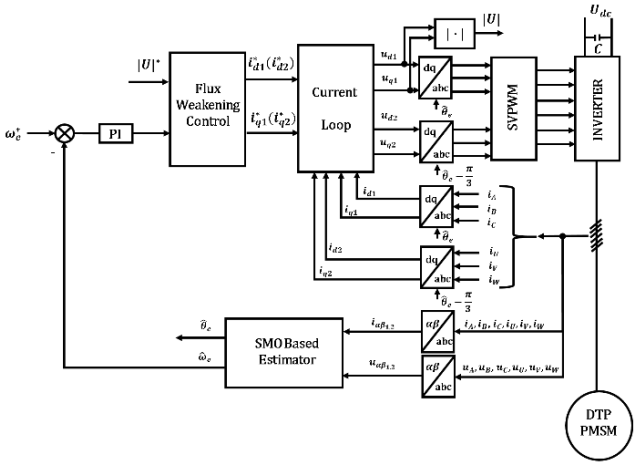


Fig. 7 Block diagram of proposed SMO based sensorless system.

## IV. Simulation Results

The block diagram of SMO based sensorless method in this study is shown in Fig. 6 and the simulation result is reported in Fig. 7.

A comparative study is made between the conventional and adaptive methods under the same working conditions, which can be roughly divided into two stages. In the first stage, the machine accelerates gradually from zero start-up to the maximum speed 18.2 krpm. There is no load during this period. The second stage starts from the end of the previous stage. During this period, the machine is controlled at the maximum speed and the load torque has a 'increase-keep-decrease' variation during 2.5-5s. Both methods are able to estimate rotor position and speed with acceptable estimation error during all the stages. Yet, there are some differences of speed and position estimation between the control performance obtained by conventional method and adaptive method. The conventional method shows greater steady state error and chattering phenomenon in speed estimation. This problem results from the phase delay caused by the low-pass filter. In the adaptive method, the low-pass filter is avoided and hence the speed estimation has less steady state error and better tracking accuracy compared to conventional method.

## V. Conclusions

The sensorless control of a symmetric DTP-PMSM (shifted by 60 electrical degrees) applied in MEA is investigated in this study. The novel contribution of this paper is the comparative study of the two SMO based estimators (conventional method and adaptive method) for the sensorless drive system. S-domain simulations are conducted to compare the effectiveness of these two methods. Compared with the conventional method, adaptive SMO method shows better tracking accuracy and lower steady state error due to the absence of the low-pass filter.

## VI. Acknowledgment

This project has received funding from the Clean Sky 2 Joint Undertaking under the European Union's Horizon 2020 research and innovation program under grant agreement No 737814.

REFERENCE

1. Levi, E., *Multiphase electric machines for variable-speed applications.* IEEE Trans. Industrial Electronics, 2008. **55**(5): p. 1893-1909.
2. Bojoi, R., et al. *Digital field oriented control for dual three-phase induction motor drives*. in *Industry Applications Conference, 2002. 37th IAS Annual Meeting. Conference Record of the*. 2002. IEEE.
3. Rottach, M., C. Gerada, and P. Wheeler. *Evaluation of motor-drive segmentation strategies for fault-tolerance*. in *ECCE Asia Downunder (ECCE Asia), 2013 IEEE*. 2013. IEEE.
4. Xu, P. and Z. Zhu, *Initial rotor position estimation using zero-sequence carrier voltage for permanent-magnet synchronous machines.* IEEE Transactions on Industrial Electronics, 2017. **64**(1): p. 149-158.
5. Fan, L., et al. *Comparative study Of back EMF based sensorless control methods for dual three-phase*

*PMSM*. in *2018 IEEE International Conference on Electrical Systems for Aircraft, Railway, Ship Propulsion and Road Vehicles & International Transportation Electrification Conference (ESARS-ITEC)*. 2018. IEEE.

6. Raca, D., et al., *Carrier-signal selection for sensorless control of PM synchronous machines at zero and very low speeds.* IEEE Transactions on Industry Applications, 2010. **46**(1): p. 167-178.

7. Qiao, Z., et al., *New sliding-mode observer for position sensorless control of permanent-magnet synchronous motor.* IEEE Transactions on Industrial electronics, 2013. **60**(2): p. 710-719.

8. Dienes, P., *The Taylor series: an introduction to the theory of functions of a complex variable*. 1957: Dover New York, NY.